# Particle size effects on interplay between charge ordering and magnetic properties in nanosized $La_{0.25}Ca_{0.75}MnO_3$

T. Zhang, T. F. Zhou, T. Qian, and X. G. Li*
*Hefei National Laboratory for Physical Sciences at Microscale and Department of Physics, University of Science and Technology of China, Anhui, Hefei 230026, China and International Center for Materials Physics, Academia Sinica, Shenyang 110015, China*

(Received 5 March 2007; revised manuscript received 26 June 2007; published 8 November 2007)

The charge ordering (CO) and magnetic properties of $La_{0.25}Ca_{0.75}MnO_3$ compounds with average particle sizes ranging from 40 to 2000 nm have been studied. With decreasing particle size, the CO transition gradually shifts to lower temperature and becomes increasingly wide and weak; meanwhile, the ferromagnetic cluster glass state appears, and the temperature $T_G$ for the appearance of ferromagnetic clusters shows a nonmonotonous variation with a maximum at about 100 nm. The magnetization at low temperature shows a relatively complex change with particle size. A core-shell model was proposed to explain these anomalous behaviors, and the temperature-particle size phase diagram of $La_{0.25}Ca_{0.75}MnO_3$ was established. These results are helpful in deeply understanding the coupling between charge and spin degrees of freedom in manganites.

DOI: 10.1103/PhysRevB.76.174415 PACS number(s): 75.47.Lx

## I. INTRODUCTION

The charge ordering (CO) in doped perovskite manganite $R_xA_{1-x}MnO_3$ ($R$ and $A$ represent rare earth elements and divalent alkaline earth elements, respectively), characterized by an ordering of the $Mn^{3+}$ and $Mn^{4+}$ species within the $MnO_2$ plane, causes the localization of $e_g$ electrons and the antiferromagnetic (AFM) spin ordering below the CO transition temperature $T_{CO}$. The CO phenomenon represents one of the most interesting issues in these materials due to the strong interactions among the charge, spin, orbital, and lattice degrees of freedom and has been studied intensively.[1–7] It has been demonstrated that the CO state can be controlled by an internal or external perturbation which varies the interplay of various degrees of freedom. For example, the substitution of Fe for Mn in charge-ordered $La_{0.33}Ca_{0.67}MnO_3$ introduces non-Jahn-Teller (non-JT) impurity $Fe^{3+}$ at $Mn^{3+}$ sites and suppresses the CO by reducing the JT distortion;[8] for $Pr_{1-x}Ca_xMnO_3$ system, a high external pressure can lead to a suppression of the CO insulating pseudo-CE-type AFM state and an appearance of the charge-disordered A-type AFM state due to the increase of the bandwidth.[9,10]

Recently, we have found that a magnetic field of 12 T induces a metal-insulator transition accompanied with reappearance of ferromagnetic (FM) state around 145 K in the charge-ordered $La_{0.5}Ca_{0.5}MnO_3$ compound, which indicates that the CO state has been melted by the magnetic field. In contrast, for $La_{0.25}Ca_{0.75}MnO_3$, the CO state is very stable due to the large JT distortion and stable AFM structure; a 14 T field has almost no impact on it.[6,11] Because of the limitation of the high magnetic field and pressure techniques in magnetic and transport measurements, how the magnetic state of this material varies during the destruction of CO state is still not clear. It is believed that the stability of the CO state is strong with the collinear AFM ordering of the localized Mn moments.[5,12] For AFM materials, when their particle size is reduced to nanoscale, the uncompensated surface spins will destroy the collinear AFM configuration,[13] which, in turn, would impede the formation of the CO state.[11,14] Therefore, varying particle size can change the CO state of manganites and provide an opportunity to study the variation of magnetic state. In addition, an investigation of the particle size effects may lead to some size-related interesting physical phenomena and is helpful to more deeply understand the coupling between the charge and spin in nanosized manganites.

In this paper, we studied the size effects on the CO state and magnetic properties of $La_{0.25}Ca_{0.75}MnO_3$ compounds. It is found that the CO state is suppressed gradually and the FM cluster-glass state appears with decreasing particle size from 2000 to 40 nm. Based on these results, a phase diagram of temperature vs particle size for $La_{0.25}Ca_{0.75}MnO_3$ is constructed.

## II. EXPERIMENT

Polycrystalline samples of $La_{0.25}Ca_{0.75}MnO_3$ were prepared by sol-gel method, which is based on the esterification and polymerization reaction of ethylene glycol (EG) and ethylenediaminetetraacetic acid (EDTA). The stoichiometric amounts of $La_2O_3$, $CaCO_3$, and 50% $Mn(NO_3)_2$ solution were used as starting materials. $La_2O_3$ and $CaCO_3$ were converted into metal nitrates by adding nitric acid. These metal nitrates and excessive EDTA were dissolved in distilled water to obtain a clear solution with an initial molar ratio of La:Ca:Mn=1:3:4. The $p$H of solution was adjusted to 6–7 by adding ethylenediamine, and then an appropriate amount of EG was added to the solution. Subsequently, the solution was heated with stirring to evaporate most of the solvent water. The resultant gel precursors were decomposed at about 300 °C to obtain black precursor powder which then was separated into several parts and annealed at temperatures from 600 to 1280 °C to gain samples with different average particle sizes. The average particle sizes were characterized by field emission scan microscopy (FESEM, JEOL, JSM-6700F) and Scherrer formula. The structure characterization

 

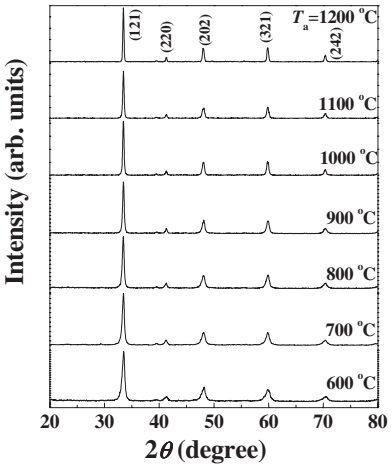


FIG. 1. The XRD patterns at room temperature of all the specimens annealed at different temperatures $T_a$.

of the samples was done by x-ray diffraction (XRD) on a MacScience MAXP18AHF diffractometer using Cu K$\alpha$ radiation. The magnetic properties were measured by a superconducting quantum interference device magnetometer. The valence $Mn^{3+}/Mn^{4+}$ ratio was determined using x-ray photoelectron spectroscopy (XPS) on the ESCA 100-VSW apparatus equipped with a Mg anode (1253.6 eV) and $K_2Cr_2O_7$ titration method.

## III. RESULTS AND DISCUSSION

The sharp diffraction peaks in the XRD patterns shown in Fig. 1 indicate the good crystallinity for each specimen without any impurity phases. With decreasing annealing temperature, the diffraction peaks become increasingly wide due to the decrease of the particle size. The clear crystal stripes belonging to (200) face of the specimen annealed at 600 °C shown in Fig. 2 also confirm the good crystallinity. Figure 3 shows the FESEM micrographs of $La_{0.25}Ca_{0.75}MnO_3$ compounds obtained by different thermal treatments. It is clearly seen that for each sample, the size of the crystallized particles is homogeneous, and the average diameter ($D$) ranges from 40 to 2000 nm as the annealing temperature increases from 600 to 1280 °C.

Figure 4 shows temperature dependences of the zero-field cooled (ZFC) and field cooled (FC) magnetizations ($M$) measured under a magnetic field of 0.01 T for the specimens with different particle sizes. For the 2000 nm sample, both the ZFC and FC magnetizations increase with decreasing temperature below 400 K, then decrease rapidly after displaying a sharp peak $P_1$ at about 240 K, signaling a development of the CO state. This feature is similar to that observed for the bulk $La_{0.25}Ca_{0.75}MnO_3$.[6,15] It is known that at high temperatures, the hopping of $e_g$ electrons between $Mn^{3+}$ and $Mn^{4+}$ ions induces a weak FM spin correlation.[14] As the temperature decreases to the onset of CO, the FM fluctuation is suppressed since the CO freezes out the hopping of $e_g$ electrons and the formation of antiferromagnetically correlated Mn spins results in a decrease of magnetization. Ac-

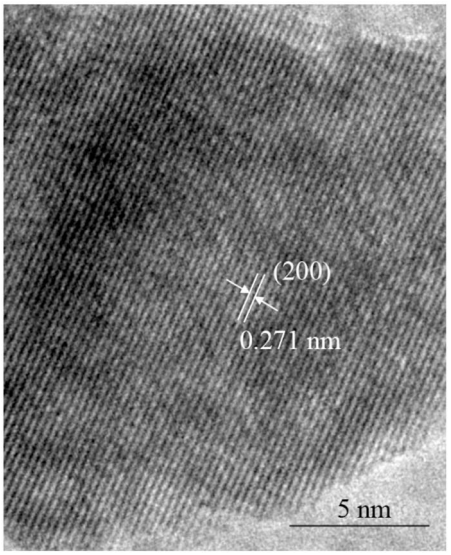


FIG. 2. The high resolution transmission electron microscopy image of the specimen annealed at 600 °C.

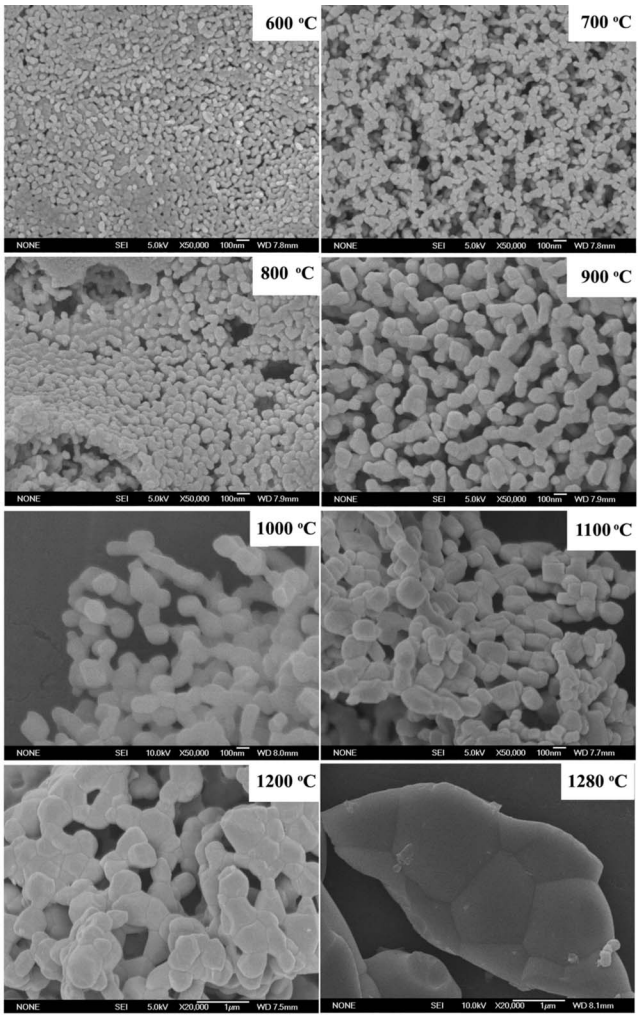


FIG. 3. FESEM micrographs of $La_{0.25}Ca_{0.75}MnO_3$ compounds obtained by different thermal treatments.

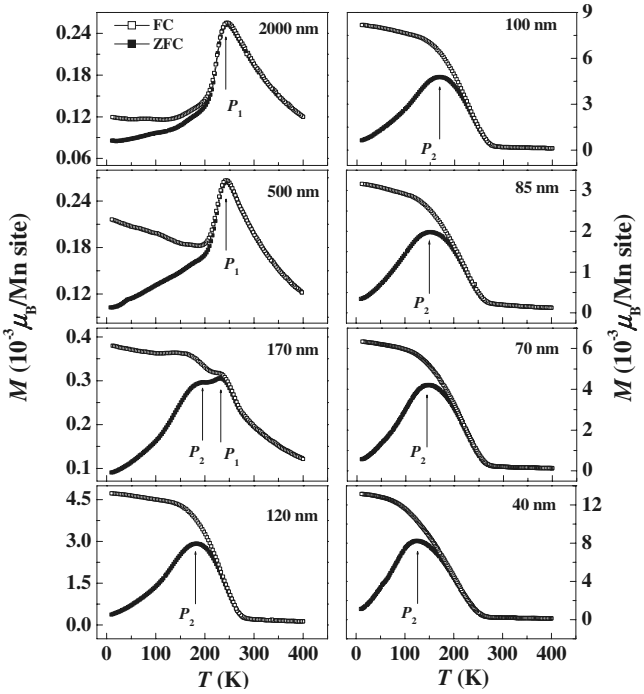


FIG. 4. Temperature dependences of the ZFC and FC magnetizations for all the specimens measured under a field of 0.01 T.

cordingly, the peak temperature of the $M$ vs $T$ curve can be defined as $T_{CO}$. For the 500 nm sample, in addition to the $P_1$ around 236 K corresponding to the CO transition, a fair upturn of the magnetization below about 174 K in the FC curve implies the reappearance of the FM fluctuations. As the particle size is reduced to 170 nm, besides $P_1$ shifting to a lower temperature and becoming indistinct, the FC magnetization exhibits a rapid increase around 200 K, whereas the ZFC curve shows another peak $P_2$ around 196 K. For the samples with particle size below 120 nm, $P_1$ disappears and $P_2$ becomes more obvious. The rapid increase in magnetization around a certain temperature in $M$ vs $T$ curves may be related to the formation of a long-range FM order or a short-range FM cluster glass.[16–19] In order to clarify the magnetic state, the ac susceptibility $\chi'(T)$ under different frequencies was measured, as plotted in Fig. 5. Obviously, the $\chi'(T)$ for 2000 and 500 nm samples is independent of frequency, and the sharp peak around $T_{CO}$ corresponds to $P_1$. When the particle size is reduced below 170 nm, the $\chi'(T)$ exhibits a strong frequency dependence, and the position $T_f$ of the peak corresponding to $P_2$ obviously shifts toward a higher temperature with increasing frequency, which confirms that the magnetic state of these specimens is of cluster-glass (CG) state at low temperatures. Therefore, the above rapid rise in magnetization is attributed to the appearance of the short-range FM coupling, forming FM clusters around a temperature $T_G$ defined as the temperature corresponding to the minimum of $dM/dT$ vs $T$ curve.[17] Upon ZFC, the FM cluster moments freeze into random orientations, and the ZFC magnetization at low temperature is much lower than the FC one in which the FM cluster moments align. With increasing temperature the frozen clusters are gradually melted, and the ZFC magnetization rises. When temperature is close to $T_G$, the FM cluster moments are strongly disturbed by thermal fluctuations and the magnetization starts to reduce, which leads to the appearance of $P_2$ in the ZFC curve. So, $P_2$ position or $T_f$ marks the defreezing temperature for CG.[18] With decreasing particle size, $T_G$ displays a nonmonotonous behavior with a maximum at about 100 nm, whereas the magnetization at low temperature shows an anomalous variation compared with $T_G$, as shown in Fig. 6. The magnetization at 10 K obtained from the ZFC $M$-$T$ curves measured with 0.01 T increases monotonously as the particle size is reduced from 2000 to 100 nm and then decreases with further decreasing size to 85 nm. However, it is surprising that the magnetization increases again below 85 nm.

The evolution of $T_G$ with particle size may be related to the following two aspects: one is the variation of the $Mn^{3+}/Mn^{4+}$ ratio,[20,21] and the other is a surface effect due to decreasing particle size. In order to clarify its origin, it is necessary to determine the $Mn^{3+}/Mn^{4+}$ value of all the samples. Figure 7 shows the typical XPS spectra of Mn $2p_{3/2}$ level of the 40, 85, 170, and 2000 nm samples. The solid

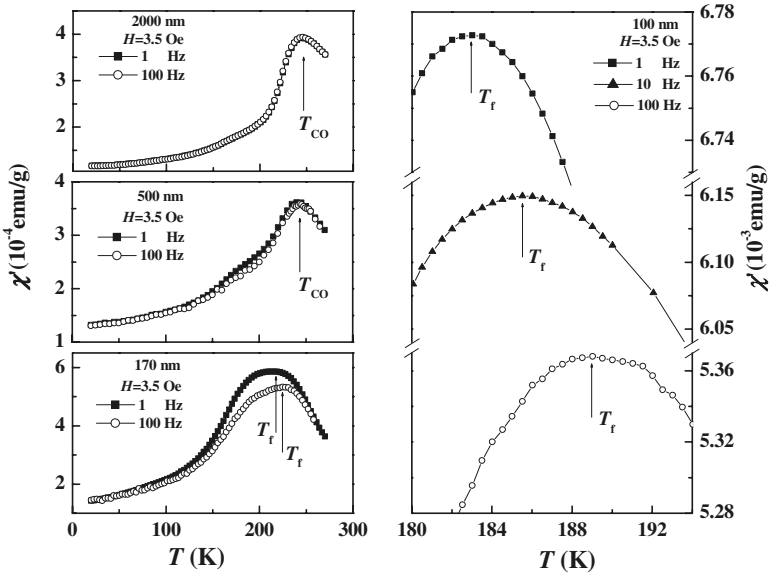


FIG. 5. Temperature dependences of the in-phase ac susceptibility in the ac magnetic field of 3.5 Oe with different frequencies.

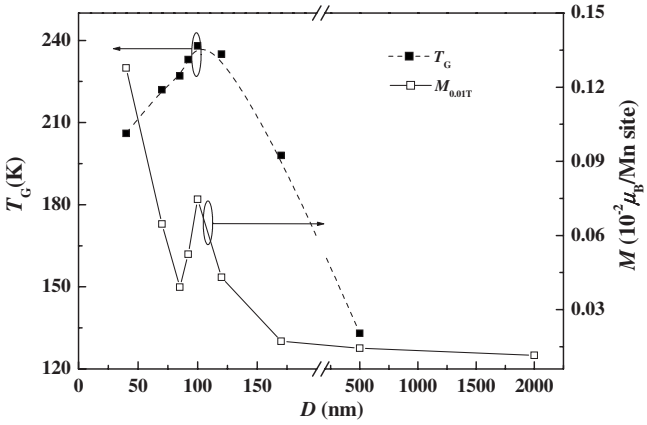


FIG. 6. Particle diameter dependences of the temperature $T_G$ for the appearance of FM clusters (left axis) and the ZFC magnetization obtained under 0.01 T ($M_{0.01\ T}$ right axis) at 10 K.

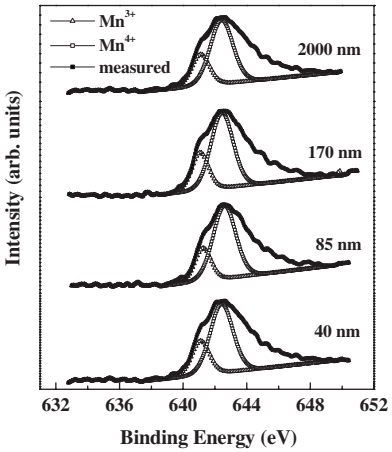


FIG. 7. Typical XPS spectra of Mn $2p_{3/2}$ level of $La_{0.25}Ca_{0.75}MnO_3$ compounds with average particle sizes of 2000, 170, 85, and 40 nm.

squares are the experimental data and the other two curves are the fitting results corresponding to $Mn^{3+}$ (open triangles) and $Mn^{4+}$ (open squares) species with binding energy values of 641.2 and 642.5 eV, respectively.[22,23] From the calculation of the internal peak areas of the two fitting curves, one can get that all the samples have almost the same $Mn^{3+}/Mn^{4+}$ value. Moreover, the titration results also show that the $Mn^{3+}/Mn^{4+}$ ratio is nearly a constant through the series (Table I). Therefore, the variation of $T_G$ with particle size should arise from the surface effect. Based on the core-shell model proposed by Bhowmik *et al.*,[24] an improved one was used to explain it, as illustrated in Fig. 8. For AFM nanoparticles, the deviation of the shell spins from a collinear AFM arrangement of the core spins leads to the uncompensated surface spins which weaken the AFM interaction across the shell and hence enhance the FM interaction [see Fig. 8(b)].[24,25] The enhanced FM coupling facilitates the formation of FM cluster glass in these regions. Under an external magnetic field, the aligned FM cluster moments lead to the macroscopical ferromagnetism and thereby the abrupt increase of the magnetization around $T_G$.[17] However, on the other hand, with further decreasing particle size, the surface spins become more disordered and thus disfavor the FM coupling.[26,27] When the two competitive factors reach a balance, the FM coupling, i.e., $T_G$ attains a maximum. Thereafter, the increasingly disordered surface spins weaken the FM coupling significantly and hence results in the decrease of $T_G$ with further decreasing particle size [Fig. 8(c)].

As for the increase of the magnetization at 10 K below 85 nm, it can be understood from the evolution of the spin configuration of an AFM nanoparticle with particle size. As aforementioned, the spins of a particle consist of core and shell spins, so the total magnetization can be given as[24]

$$M = \alpha M_{\text{shell}} \sum_{ij} \cos\theta_{ij} + (1-\alpha) M_{\text{core}}, \tag{1}$$

where the shell/core ratio $\alpha$ increases with decreasing particle size, $M_{\text{shell}}$ and $M_{\text{core}}$ represent the magnetizations of the shell and core, respectively, and $\theta_{ij}$ with $0° \leqslant \theta_{ij} \leqslant 180°$ is the angle between spins $i$ and $j$. For the core spins, $\theta_{ij}$

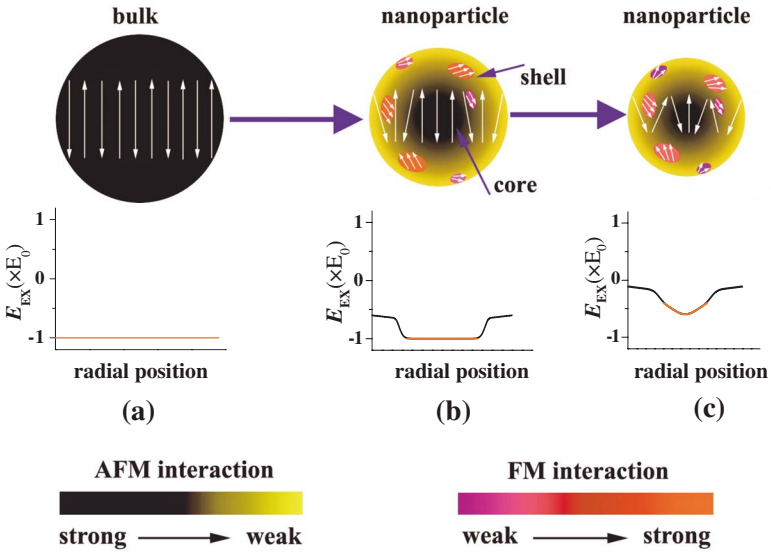


FIG. 8. (Color online) Schematic diagrams (two dimensional) of the evolution of the magnetic configuration, the exchange energy, and magnetic interactions with particle size, proposed on the basis of the core-shell model in Ref. 24. Arrows only represent the spins orientation. (a) Perfect AFM spin ordering in a bulk $La_{0.25}Ca_{0.75}MnO_3$, assuming the AFM exchange energy $E_{ex}=-E_0$. (b) For nanoparticles, the core spins are nearly antiparallel, the deviation of shell spins from AFM arrangement: makes the $E_{ex}$ value less negative and leads to the formation of FM cluster glass across the shell regions without external magnetic fields. (c) For nanoparticles with smaller particle size, the more disordered shell spins not only induce the deviation of core spins from AFM arrangement and accordingly further increase $E_{ex}$ value but also weaken the FM coupling greatly.

TABLE I. List of the particle sizes obtained by FESEM and the Scherrer formula and the $Mn^{3+}/Mn^{4+}$ ratio obtained by XPS and titration methods.

| Annealing temperature (°C) | Particle size (nm) | $Mn^{3+}/Mn^{4+}$ (XPS) | $Mn^{3+}/Mn^{4+}$ (titration) |
|---|---|---|---|
| 1280 | 2000 | 1:2.86 | 1:3.12 |
| 1200 | 500 | 1:2.84 | 1:3.16 |
| 1100 | 170 | 1:2.87 | 1:2.92 |
| 1000 | 120 | 1:2.84 | 1:2.89 |
| 900 | 100 | 1:2.88 | 1:3.11 |
| 850 | 90 | 1:2.89 | 1:2.86 |
| 800 | 85 | 1:2.87 | 1:2.78 |
| 700 | 70 | 1:2.86 | 1:3.08 |
| 600 | 40 | 1:2.91 | 1:3.13 |

$\approx 180°$, while $\theta_{ij} < 180°$ for the shell spins which are more easily polarized by an external field than the core spins; therefore, $M_{\text{shell}}$ is much larger than $M_{\text{core}}$. When more spins break their AFM (180°) configuration with increasing $\alpha$, it will lead to an enhancement of $M$. As $D < 85$ nm, $\alpha$ becomes so large that the enhanced magnetization resulting from the shell spins prevails over the reduced one resulting from the weakened FM coupling by the disordered shell spins, and thus leads to the increase of macroscopic magnetization.

The aforementioned magnetic properties as a function of particle size are further evidenced by the $M$ vs $H$ curves at 10 K shown in Fig. 9. With decreasing particle size, the curves gradually show a FM characteristic as indicated by the hysteresis loop of the 100 nm sample in the inset of Fig. 9, and the magnetization at 5 T increases by about 318% with decreasing particle size from 2000 to 40 nm. It should be noted that the magnetization value of 0.18 $\mu_B$/Mn site under 5 T for 40 nm is much smaller than the ideal one (3.25 $\mu_B$/Mn site, provided that all the Mn ions have FM ordering). This implies that CO and AFM coexist in most regions of the samples at low temperatures. However, there

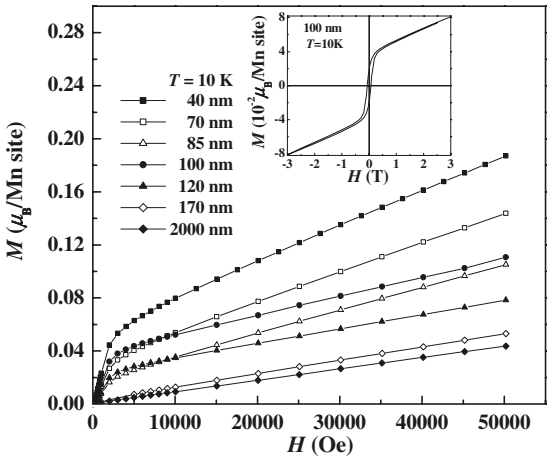


FIG. 9. Magnetic field dependences of the magnetizations for $La_{0.25}Ca_{0.75}MnO_3$ samples at 10 K. Inset: The hysteresis loop at 10 K for the 100 nm sample.

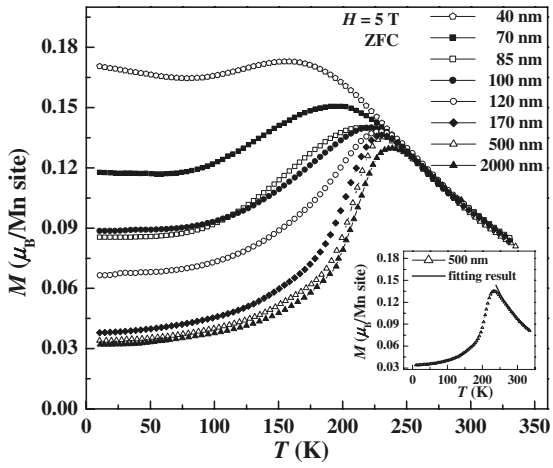


FIG. 10. Temperature dependences of the ZFC magnetizations for all the samples measured under 5 T. Inset: An example of good fitting result using Curie-Weiss law at high temperatures for the 500 nm sample.

is no clear evidence for CO transition observed in the $M$ vs $T$ curves under low field for $D \leqslant 120$ nm. This can be ascribed to the dissimilar sensitivities of different magnetic phases to applied magnetic fields. It is well known that the FM cluster moments are easily polarized under low fields, while the AFM and paramagnetism susceptibilities are much lower, which induces that the characteristic of the CO transition is covered up for the samples with particle size below 120 nm due to the existence of the FM clusters under 0.01 T. With increasing field, the FM cluster moments saturate rapidly, while the AFM moment still increases linearly (see Fig. 9), and it can be anticipated that the characteristic of the CO transition should become gradually visible under high magnetic fields. Therefore, in order to further observe the effect of particle size on the CO state, it is necessary to study the $M$ vs $T$ curves under a higher magnetic field, as shown in Fig. 10. For all the samples, the susceptibilities at high temperatures follow the Curie-Weiss law, and a good fitting result of the 500 nm sample at high temperatures is shown in the inset of Fig. 10. With decreasing temperature, the ZFC curve shows a distinct maximum at a certain temperature. This characteristic is similar to that of a bulk material[28] and reveals that there exists a CO transition for all the samples. It is notable that, with decreasing particle size, $T_{\text{CO}}$ gradually shifts to a lower temperature and the transition width becomes increasingly wide due to the weakening of the CO state. This CO state suppression is actually related to the uncompensated surface spins. According to Heisenberg exchange theory, the exchange energy $E_{\text{ex}}$ between two neighboring spins is expressed as[24]

$$E_{\text{ex}} \propto -J_{\text{ex}} \sum_{ij} S_i S_j \cos \theta_{ij}, \tag{2}$$

where $J_{\text{ex}}$ is an exchange constant and $S_i$ and $S_j$ represent the spin quantum number of the spins $i$ and $j$, respectively. For a bulk material, one can assume $\theta_{ij} = 180°$ and $E_{\text{ex}} = -E_0$, as illustrated in Fig. 8(a). For nanoparticles, although the core spins are almost antiparallel, i.e., $\theta_{ij} \approx 180°$, the deviation of

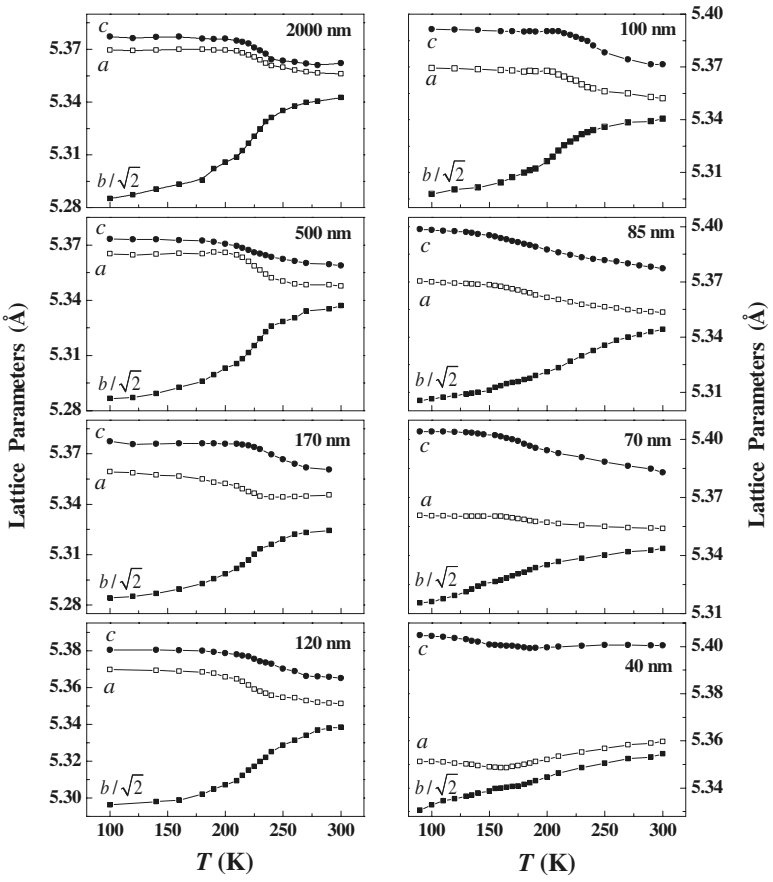


FIG. 11. Lattice parameters $a$, $b/\sqrt{2}$, and $c$ for all the $La_{0.25}Ca_{0.75}MnO_3$ samples as a function of temperature. The lines are guides for the eyes.

shell spins from the AFM arrangement makes $-E_0 < E_{ex} < 0$ across the shell regions, as schematically shown Figs. 8(b) and 8(c), and thereby enhances the surface energy.[29] In addition, the increasing surface strain resulting from the surface defects also raises the surface energy.[14] As a result, the destruction of collinear AFM configuration and the enhanced surface energy suppress the CO.[12,14] Meanwhile, the FM clusters appear due to the double exchange interaction between $Mn^{3+}$ and $Mn^{4+}$ cation.

The suppression of the CO state is further confirmed by the temperature dependences of orthorhombic lattice parameters $a$, $b/\sqrt{2}$, and $c$, obtained by analyzing the powder XRD patterns using the Rietveld refinement method based on the space group *Pnma* for all samples, as shown in Fig. 11. It is seen that a dramatic change of the lattice parameters near $T_{CO}$ gradually shifts to a lower temperature with decreasing particle size and becomes increasingly flat, which verifies the suppression of the CO state.

Based on the magnetization measurements and the structure analysis, a phase diagram of temperature vs particle size for $La_{0.25}Ca_{0.75}MnO_3$ is constructed, as shown in Fig. 12. The solid squares and open circles represent the $T_G$ determined under 0.01 T and $T_{CO}$ obtained under 5 T, respectively. With decreasing particle size, $T_G$ firstly increases and then decreases after reaching a maximum at about 100 nm, while $T_{CO}$ monotonically decreases. It can be predicted that when the particle size is below a critical value ($D_0$), the disordered surface spins will cause a fundamental change in the magnetic configuration throughout a particle via exchange coupling[25] and make the surface energy be comparable with the CO energy (see Fig. 8), which will lead to a complete disappearance of the CO state.[14] $D_0$ can be obtained by the empirical equation

$$T_{CO}(D) = T_{CO}^{b}\left(1 - \frac{D_0}{D}\right)^{\gamma}, \tag{3}$$

where $T_{CO}^{b}$ is the CO transition temperature of the bulk material, $D_0$ is the critical particle size for the disappearance of the CO sate, and $\gamma$ is a fitting parameter. The solid line in

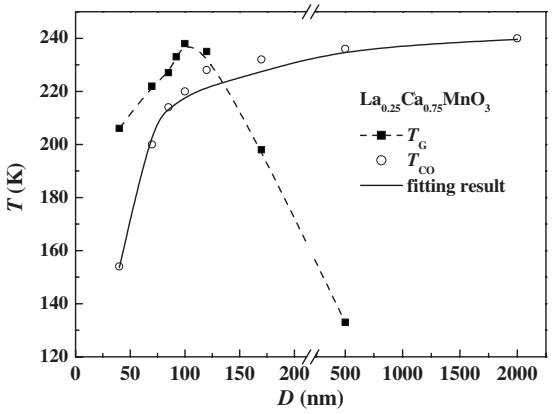


FIG. 12. A temperature vs particle size phase diagram of $La_{0.25}Ca_{0.75}MnO_3$. The solid line is the fitting result using Eq. (3). The dashed line is a guide for the eyes.

Fig. 12 is the fitting result with $T_{CO}^{b}=241$ K, $D_0=17$ nm, and $\gamma=0.54$.

## IV. CONCLUSION

In summary, with decreasing particle size, the robust charge ordering in the bulk $La_{0.25}Ca_{0.75}MnO_3$ compound is weakened, accompanied with an appearance of a FM cluster-glass state. Moreover, the temperature $T_G$ for the appearance of FM clusters firstly increases and then decreases after reaching a maximum at about 100 nm, while the magnetization at low temperature shows a maximum and a minimum around 100 and 85 nm, respectively. These results can be attributed to the surface spins which gradually change the magnetic configuration of the particle via exchange coupling and magnetic interactions with decreasing particle size. It can be predicated that when the particle size is reduced to a critical value $D_0$, the charge ordering will completely disappear.

## ACKNOWLEDGMENTS

This work was supported by the National Natural Science Foundation of China (No. 50421201 and No. 10334090) and the National Basic Research Program of China (No. 2006CB922005).

*Corresponding author; lixg@ustc.edu.cn

[1] E. Dagotto, T. Hotta, and A. Moreo, Phys. Rep. **344**, 1 (2001).
[2] M. B. Salamon and M. Jaime, Rev. Mod. Phys. **73**, 583 (2001).
[3] C. N. R. Rao, A. Arulraj, A. K. Cheetham, and B. Raveau, J. Phys.: Condens. Matter **12**, R83 (2000).
[4] V. Hardy, A. Maignan, S. Hébert, and C. Martin, Phys. Rev. B **67**, 024401 (2003).
[5] M. Tokunaga, N. Miura, Y. Tomioka, and Y. Tokura, Phys. Rev. B **57**, 5259 (1998).
[6] T. Qian, R. K. Zheng, T. Zhang, T. F. Zhou, W. B. Wu, and X. G. Li, Phys. Rev. B **72**, 024432 (2005).
[7] W. Prellier, E. R. Buzin, Ch. Simon, B. Mercey, M. Hervieu, S. de Brion, and G. Chouteau, Phys. Rev. B **66**, 024432 (2002).
[8] T. S. Orlova, J. Y. Laval, P. Monod, J. G. Noudem, V. S. Zahvalinskii, V. S. Vikhnin, and Y. P. Stepanov, J. Phys.: Condens. Matter **18**, 6729 (2006).
[9] D. P. Kozlenko, Z. Jirák, I. N. Goncharenko, and B. N. Savenko, J. Phys.: Condens. Matter **16**, 5883 (2004).
[10] C. W. Cui and T. A. Tyson, Phys. Rev. B **70**, 094409 (2004).
[11] X. G. Li, R. K. Zheng, G. Li, H. D. Zhou, R. X. Huang, J. Q. Xie, and Z. D. Wang, Europhys. Lett. **60**, 670 (2002); X. G. Li, H. Chen, C. F. Zhu, H. D. Zhou, R. K. Zheng, and J. H. Zhang, Appl. Phys. Lett. **76**, 1173 (2000).
[12] R. Y. Gu, Z. D. Wang, and C. S. Ting, Phys. Rev. B **67**, 153101 (2003).
[13] R. H. Kodama, S. A. Makhlouf, and A. E. Berkowitz, Phys. Rev. Lett. **79**, 1393 (1997).
[14] M. Pissas, I. Margiolaki, K. Prassides, and E. Suard, Phys. Rev. B **72**, 064426 (2005).
[15] R. K. Zheng, R. X. Huang, A. N. Tang, G. Li, X. G. Li, J. N. Wei, J. P. Shui, and Z. Yao, Appl. Phys. Lett. **81**, 3834 (2002).
[16] J. Wu and C. Leighton, Phys. Rev. B **67**, 174408 (2003).
[17] S. Mukherjee, R. Ranganathan, P. S. Anilkumar, and P. A. Joy, Phys. Rev. B **54**, 9267 (1996).
[18] X. G. Li, X. J. Fan, G. Ji, W. B. Wu, K. H. Wong, C. L. Choy, and H. C. Ku, J. Appl. Phys. **85**, 1663 (1999).
[19] D. A. Pejakovic, J. L. Manson, J. S. Miller, and A. J. Epstein, J. Appl. Phys. **87**, 6028 (2000).
[20] Y. G. Zhao, R. Fan, X. P. Zhang, H. Balci, S. B. Ogale, T. Venkatesan, T. K. Mandal, and J. Gopalakrishnan, J. Magn. Magn. Mater. **284**, 35 (2004).
[21] D. Niebieskikwiat, A. Caneiro, and R. D. Sánchez, J. Appl. Phys. **93**, 8080 (2003).
[22] S. Ponce, M. A. Peńa, and J. L. G. Fierro, Appl. Catal., B **24**, 193 (2000).
[23] E. Beyreuther, S. Grafstrom, L. M. Eng, C. Thiele, and K. Dorr, Phys. Rev. B **73**, 155425 (2006).
[24] R. N. Bhowmik, R. Nagarajan, and R. Ranganathan, Phys. Rev. B **69**, 054430 (2004).
[25] A. Punnoose, H. Magnone, M. S. Seehra, and J. Bonevich, Phys. Rev. B **64**, 174420 (2001).
[26] T. Zhang, G. Li, T. Qian, J. F. Qu, and X. G. Li, J. Appl. Phys. **100**, 094324 (2006).
[27] S. S. Rao, S. Tripathi, D. Pandey, and S. V. Bhat, Phys. Rev. B **74**, 144416 (2006).
[28] H. Woo, T. A. Tyson, M. Croft, S. W. Cheong, and J. C. Woicik, Phys. Rev. B **63**, 134412 (2001).
[29] S. Dong, F. Gao, Z. Q. Wang, J. M. Liu, and Z. F. Ren, Appl. Phys. Lett. **90**, 082508 (2007).